



**HAL**  
open science

# An Oatp transporter-mediated steroid sink promotes tumor-induced cachexia in *Drosophila*

Paula Santabárbara-Ruiz, Pierre Léopold

► **To cite this version:**

Paula Santabárbara-Ruiz, Pierre Léopold. An Oatp transporter-mediated steroid sink promotes tumor-induced cachexia in *Drosophila*. *Developmental Cell*, 2021, 56 (19), pp.2741-2751.e7. 10.1016/j.devcel.2021.09.009 . hal-03979469

**HAL Id: hal-03979469**

**<https://hal.science/hal-03979469>**

Submitted on 16 Oct 2023

**HAL** is a multi-disciplinary open access archive for the deposit and dissemination of scientific research documents, whether they are published or not. The documents may come from teaching and research institutions in France or abroad, or from public or private research centers.

L'archive ouverte pluridisciplinaire **HAL**, est destinée au dépôt et à la diffusion de documents scientifiques de niveau recherche, publiés ou non, émanant des établissements d'enseignement et de recherche français ou étrangers, des laboratoires publics ou privés.



Distributed under a Creative Commons Attribution - NonCommercial 4.0 International License

# An Oatp transporter-mediated steroid sink promotes tumor-induced cachexia in *Drosophila*

Paula Santabárbara-Ruiz and Pierre Léopold\*<sup>1</sup>

Institut Curie, PSL Research University, CNRS UMR3215, INSERM U934, UPMC Paris-Sorbonne, 26 Rue d'Ulm, 75005, Paris, France.

\*correspondence : pierre.leopold@curie.fr, <sup>1</sup>lead contact

## Summary

Cancer cachexia is associated with many types of tumors and characterized by a combination of anorexia, loss of body weight, catabolic alterations and systemic inflammation. We developed a tumor model in *Drosophila* larvae causing cachexia-like syndrome and found that cachectic larvae show reduced levels of the circulating steroid ecdysone (Ec). Artificially importing Ec in the tumor using the Ecl/Oatp74D importer aggravated cachexia, while feeding animals with ecdysone rescued cachectic defects. This suggested that a steroid sink induced by the tumor promotes catabolic alterations in healthy tissues. We found that Oatp33Eb, a member of the Oatp transporter family, is specifically induced in tumors promoting cachexia. Overexpression of Oatp33Eb in non-cachectic tumors induced cachexia, while its inhibition in cachectic tumors restored circulating Ec and reversed cachectic alterations. Oatp transporters are induced in several types of hormone-dependent tumors, suggesting that a similar sink effect could modify hormonal balance in cachectic cancer patients.

## Key words

Tumor, cancer, cachexia, tissue wasting, *Drosophila*, Ecdysone, steroid hormones, Oatp33Eb, SLCO transporters.

## Introduction

Cachexia is a devastating tumor-induced metabolic disorder marked by a progressive wasting of adipose and muscle tissues. This is driven by a combination of reduced food intake, insulin resistance, excess catabolism and inflammation. Cachexia greatly impacts the quality of life of patients, reduces the efficacy of chemotherapy and increases susceptibility to infections. This condition is often poorly diagnosed and very few opportunities for treatment are offered (Fearon, Arends and Baracos, 2013).

Rodent models have provided important contributions to our understanding of cancer cachexia (Bennani-Baiti and Walsh, 2011; Molino *et al.*, 2019). They established a role for two major groups of pro-catabolic agents: (i) tumor-produced factors (pro-inflammatory cytokines, proteolysis-inducing factors and lipid mobilizing factors) and (ii) host factors, mainly pro-inflammatory cytokines.

In parallel, patient studies have highlighted an important hormonal imbalance associated with the cachectic syndrome. Cachectic patients usually present high GH and low IGF-I levels, suggesting a state of GH resistance (Honors and Kinzig, 2012). Insulin resistance is also frequently observed in these patients. Finally, hypogonadism is found associated with cachexia in men and lower circulating testosterone correlates with reduced muscular mass. The increase in catabolic processes suggests that cachexia could at least partially result from a reduction of general anabolic factors, and motivated the use of hormone replacement therapies. However, the molecular mechanisms responsible for these hormonal perturbations remain to be elucidated, and are needed for novel therapeutic approaches.

Several *Drosophila* tumor models have recently been used to study cancer-induced cachexia, taking advantage of the conservation with vertebrates of both the pathways regulating tumor growth and the hormonal physiology (Brumby and Richardson, 2005; Leopold and Perrimon, 2007; Droujinine and Perrimon, 2016). The main advantages of these genetically engineered fly models is that the tumor and the host can be modified in parallel, giving the opportunity to study intricate tumor-host interactions.

In the adult fly, several tumor-produced factors have been defined as cachectic inducers, such as the IGF-binding protein (IGFBP) homolog ImpL2 and the PDGF/VEGF homolog Pvr1 (Figueroa-Clarevega and Bilder, 2015; Kwon *et al.*, 2015; Song *et al.*, 2019). However, the adult fly model presents some limitations due to the technical difficulty to perform tumor injections avoiding an immune challenge and controlling the quantity of injected tissue, or the possible bias of generating tumors in organs essential for animal physiology.

An alternative is to observe metabolic alterations in larvae developing epithelial tumors in non-essential tissues such as the wing or eye imaginal discs. Larval physiology relies on conserved hormonal relays like insulin-like peptides, glucagon-like hormones and steroids (Ecdysone, henceforth Ec), which make it a particularly suited system to study how tumor development impairs general metabolic homeostasis and hormonal balance.

In the current work, we use a larval model of tumor-induced cachexia to study the role of hormone imbalance in this process. Cachectic, tumor-bearing animals show an important reduction of circulating steroids (Ec) and a state of insulin resistance, suggesting a conserved hormonal imbalance. Artificially inducing steroid import in tumor cells by expressing the ecdysteroid transporter Oatp74D (also called Ecl) aggravates the proportion of cachectic animals without increasing tumor burden. Conversely, feeding cachectic animals with ecdysone-containing food rescues cachexia. Oatp33Eb, another member of the Oatp transporters (and not other family members), is specifically induced in cachectic tumors, and the overexpression of this gene exacerbates cachexia as well. Its knockdown in the tumor restores normal levels of circulating Ec and rescues all cachectic symptoms, while maintaining tumor growth.

We therefore propose a model whereby tumors induce cachectic symptoms by uptaking circulating steroids at the expense of healthy tissues. This “sink effect” leads to a catabolic switch as observed in muscles and fat. Remarkably, some members of the OATP family of transporters are induced in human tumors prone to cachectic evolution, opening the possibility to use this mechanism of steroid uptake as an early marker or a therapeutic target of cancer-induced cachexia.

## Results

### Tumor-induced cachexia triggers hormonal imbalance in *Drosophila* larvae

To explore *in vivo* the role of hormonal imbalance in tumor-induced cachexia, we used *Drosophila* larvae as a fast and reproducible model that recapitulated several of the pathophysiological mechanisms observed in the human syndrome. To this aim, we induced tumor using the flip-out technique (Pagliarini and Xu, 2003 - see methods) in the eye imaginal disc, a non-essential tissue with no described physiological function during larval life. The combination of an oncogenic *ras*<sup>V12</sup> mutation with an RNA interference silencing the tumor-suppressor gene *disc large* (*dlg*<sup>RNAi</sup>) induces aggressive eye tumors. After 3 days, we observe cachectic symptoms in a fraction of the larval population. Cachectic larvae present an accumulation of body fluid (bloating syndrome), body weight loss, fat and muscle tissue wasting, and a perturbation of feeding behavior (anorexia) (Fig. 1A-G, Suppl. Fig. 1A-E). In addition, we observed that the fat body (the functional equivalent to mammalian adipose tissue and liver) of cachectic animals responds poorly to insulin stimulation (Fig. 1H, Suppl. Fig. 1F). This, together with high blood glucose, insulinemia and reduced glucose uptake by fat body cells (Fig. 1I-J, Suppl. Fig. 1F), defines a state of insulin resistance, as described in cancer cachexia. Apart from the eye imaginal discs, *eye-Gal4* drives GFP expression in a subset of cells in the optic lobe but, when used in our tumor model together with *elav.Gal80* or *syb.Gal80*, the percentage of cachectic larvae did not vary (Suppl. Fig. 2A-D). Notably, *Impl2*, a recently described cachectic inducer interfering with insulin response was upregulated in tumors, but its inhibition did not rescue cachexia (Suppl. Fig. 3A, B).

The steroid hormone ecdysone (Ec) plays key roles during *Drosophila* development both as an anabolic hormone and a timer of developmental transitions (Yamanaka, Rewitz and O'Connor, 2013). We first noticed that Ec signaling was upregulated in cachectic tumors compared with non-cachectic ones from the same genotype (Fig. 2A-E). These animals present an upregulation of *Dilp8* and 6hr delay at the larva-pupa transition (Suppl. Fig. 3C,D). Since *Dilp8* could inhibit ecdysone production, we tested the effect of silencing *Dilp8* in the tumor on the developmental delay and cachexia. In these conditions, although the developmental delay was rescued, the prevalence of cachexia was only mildly reduced (Suppl. Fig. 3A,D), suggesting that *Dilp8* plays a minor role in cachectic induction. Tumor-bearing cachectic larvae present a strong reduction of total circulating ecdysteroids compared to tumor-bearing, non-cachectic animals

(Fig. 2F). The increase in hemolymph volume observed in cachectic larvae further contributes to reducing concentrations of circulating ecdysteroids available to peripheral tissues. We did not observe differences in the levels of expression of the “Halloween” group of ecdysteroidogenic enzymes in cachectic animals (Suppl. Fig. 3E), and PTTH and Serotonin circuitries were intact in the tumor-bearing larvae (Suppl. Fig. 3F), suggesting that ecdysone synthesis is not modified by the presence of the tumor. Therefore, the reduction of Ec levels in cachectic larvae could be attributed to another mechanism. To test this hypothesis, we forced ecdysone uptake in the tumor by inducing the expression of *Ecl*, a member of the *Oatp* transporter family recently shown to specifically import ecdysone in *Drosophila* cells (also called *Oatp74D*, Okamoto *et al.*, 2018). Although neither tumor burden nor aggressiveness were significantly modified in these conditions, the percentage of cachectic animals increased from 27% to 85% (compare *tumor>* and *tumor>Ecl*, Fig. 1A-J, Suppl. Fig. 1A-F, Suppl. Fig. 3G), correlating with a reduction of circulating ecdysone in the general population of tumor-bearing larvae (Fig. 2F). By contrast, when intra-tumor EcR signaling was artificially upregulated by silencing the ecdysone-degrading enzyme *Cyp18a1* (*tumors>Cyp18a1<sup>RNAi</sup>*), the fraction of cachectic animals did not change, nor did the tumor burden (Suppl. Fig. 2C,E-G). This indicates that the critical parameter to promote cachexia is the flux of ecdysone in the tumor, and that intra-EcR signaling is not relevant. Tumors with elevated EcR signaling are not over-proliferating, suggesting that tumor cells have become insensitive to the anabolic effects of Ec for growth and proliferation. Conversely, blocking ecdysone signaling in the tumor (*tumor>EcR<sup>DN</sup>*, *tumor>shd<sup>RNAi</sup>* and *tumor>Cyp18a1*, see methods) rescued circulating levels of ecdysone as well as cachexia, suggesting that a positive feedback mechanism involving intra-cellular EcR signaling controls ecdysone uptake by the tumor (Fig. 1A-J, Suppl. Fig. 1A-F, Suppl. Fig. 3H).

In conclusion, a fraction of tumor-bearing larvae presents cachectic symptoms associated with hormonal imbalance, including a strong reduction of circulating steroids. Increasing ecdysone uptake by the tumor correlates with a reduction of circulating levels and aggravates the cachectic effect without affecting tumor growth or aggressiveness. This suggests that the catabolic switch observed in non-tumorous tissues could be due to an ecdysone “sink effect” induced by the tumor.

### **Ecdysone uptake by the tumor causes a decrease in ecdysone signaling in healthy tissues**

The consequence of a sink effect would be a reduction of ecdysone signaling in peripheral tissues. To test this, we quantified Ecdysone receptor (EcR) activity using the reporter EcREGFP (Kimura *et al.*, 2008) in fat body cells. Indeed, the level of GFP fluorescence in the fat body of tumor-bearing animals (*tumor>*) is reduced compared to no tumor-bearing ones (Fig. 2G, H). The quantification shows a further decrease of EcREGFP in *tumor>Ecl*, and a rescue in *tumor>EcR<sup>DN</sup>*. We also observed a significant reduction of nuclear EcR accumulation in the fat body of cachectic animals (Fig. 2I, J). This was confirmed by analyzing the level of direct targets of EcR like *broad* and *E78*, which show a reduction in *tumor>* and *tumor>Ecl*

conditions (Fig. 2K). Therefore, variations in circulating E correlate with the level of EcR signaling in peripheral tissues, and Ec uptake by the tumor limits ecdysone signaling in peripheral tissues.

We then tested whether supplementing 20-E, the active form of Ec, in the food would rescue the cachectic phenotype. Although 20-E feeding did not modify the tumor burden or aggressiveness, it efficiently rescued cachexia in *tumor>* and *tumor>Ecl* conditions (Fig. 3A-G, Suppl. Fig. 4). Conversely, feeding animals with a food medium lacking ergosterol (a precursor of ecdysone that is no longer produced by the *erg2Δ* yeast strain) strongly increased the proportion of cachectic animals despite a reduced tumor burden (Fig. 3H-O, Suppl. Fig. 5). Remarkably, although *tumor>EcR<sup>DN</sup>* animals did not show cachexia in normal food, they all presented bloating in *erg2Δ* food (Fig. 3H-O, Suppl. Fig. 5). This indicates that the reduction of circulating steroid is the main trigger for inducing cachexia in tumor-bearing larvae.

#### **The transporter *Oatp33Eb* is upregulated in the tumor and drives the sink effect.**

Since *Ecl* drives Ec uptake in the tumors when over-expressed, we checked if it could be upregulated in tumorous discs, but this is not the case (Fig. 4A). Moreover, silencing *Ecl* in the tumor did not rescue cachectic syndromes (Fig. 4B, Suppl. Fig 6A), indicating that *Ecl* is not responsible for the sink effect. Seven other *Oatp*-encoding genes are present in the fly genome and we compared their expression in normal and tumorous discs. Only *Oatp33Eb* was found upregulated in tumors, and specifically in cachectic ones (Fig. 4A,J). When targeted to tumor cells, *Oatp33Eb-RNAi* (and no other *Oatp-RNAi* constructs) could prevent cachexia without modifying the tumor burden or aggressiveness (Fig. 4A-J). Conversely, overexpression of the *Oatp33Eb* gene in tumors aggravated the fraction of cachectic animals, similar to *Ecl* overexpression (Fig. 4A-J, Suppl. Fig 6 A-D, compare with Fig. 1). The *Oatp33Eb* protein localizes at the cell membrane, as shown by immunostaining of *tumors>Oatp33Eb-Flag-HA* (Fig. 4K).

Ec signaling was upregulated in *tumors>Oatp33Eb* compared to non-cachectic tumors and was strongly decreased in *tumors>Oatp33Eb<sup>RNAi</sup>* (Fig. 5A-C). Conversely, EcR target gene levels and anti-EcR immunostaining were strongly decreased in fat body cells of *tumors>Oatp33Eb* animals, and increased in *tumor>Oatp33Eb<sup>RNAi</sup>* animals (Fig. 5D-F). Accordingly, the levels of circulating ecdysteroids were restored by suppressing *Oatp33Eb* expression in tumors (Fig. 5G). Therefore, the induction of *Oatp33Eb* by cachectic tumors is responsible for the observed sink effect and the tumor-induced cachectic syndrome. We found that *shade* expression is not significantly modified in tumors, suggesting that their ability to convert Ec into active 20E is not altered (Suppl. Fig 6E).

*tumor>Oatp33Eb<sup>RNAi</sup>* larvae are slightly advanced compared to *tumor>* larvae and still produced Dilp8 (Suppl. Fig 6F,G). PTTH nor Serotonin circuitries showed morphological differences and

ecdysteroidogenic gene expression is not altered in *tumor>Oatp33Eb<sup>RNAi</sup>* (Suppl. Fig 6H,I). In *tumors>Oatp33Eb*, *ecd*, *dare*, *mld* and *wok* were significantly downregulated (Suppl. Fig 6I).

Several *Drosophila* tumor models exist using various genetic backgrounds both in larval and adult contexts (Sonoshita and Cagan, 2017) . We therefore wondered if *Oatp* genes could participate in promoting cachexia in different tumor and host environments. Interestingly, *Ecl* or *Oatp33Eb* overexpression in a non-cachectic tumor model (*rn>avl<sup>RNAi</sup>*) efficiently triggered cachexia (Fig. 5H-K). Additionally, cachexia was aggravated in *pdm2>yki<sup>SA</sup>* tumor-bearing larvae (Suppl. Fig. 7A-D). We then tested the role of *Oatp33Eb* in adult cachexia by injecting tumor explants in the abdomen of adult females. While females efficiently bloated 12 days after injection of *Ras<sup>V12</sup>/dlg<sup>RNAi</sup>* tumor explants (Fig. 5L), suppressing *Oatp33Eb* expression in tumor explants significantly reduced bloating prevalence (Fig. 5M) and increased the longevity of injected flies (Fig. 5N). *Ecl* and *Oatp33Eb* were normally expressed in non-cachectic tumors (*nub>Ras<sup>V12</sup>*, *nub>Ecl*, *nub>Cyp18ai1<sup>RNAi</sup>* and *rn>avl<sup>RNAi</sup>*, Suppl. Fig. 7E-H), while upregulated in cachectic *dlg<sup>Y</sup>* mutant larvae (Suppl. Fig.7I).

Finally, as suggested by rescue experiments using *EcR<sup>DN</sup>* expression in the tumor (see our Fig. 1), we found that inhibition of EcR signaling (*tumor>EcR<sup>DN</sup>*) prevents *Oatp33Eb* upregulation observed in tumor cells (Fig. 4J) indicative of a positive feedback loop on *Oatp33Eb* expression exerted by EcR signaling in a tumor context. In line with this, numerous putative EcR/Usf binding sites are present in the promoter region of the *Oatp33Eb* gene (Suppl. Fig. 8A).

*Oatp* transporters are conserved in human (*solute carrier organic anion -SLCO-* gene family) and were previously shown to transport xenobiotics and drugs such as anticancer agents, and possibly hormones (Obaidat, Roth and Hagenbuch, 2012). Searching the *TGCA* database, we found that some of the *SLCO* genes are preferentially expressed in tumors with high prevalence of cachexia (advanced head and neck, 57% prevalence; lung non-small cell, 36% prevalence; pancreatic, 40-54% prevalence; colorectal, 28% prevalence; breast, 30% prevalence; prostate, 50% prevalence) (Suppl. Fig. 8B). *SLCO1B3*, *SLCO1B1* and *SLCO1B7*, the most upregulated genes of the family, show highest similarity (40%) with *Drosophila Oatp33Eb* (Suppl. Fig. 8C). This and our findings in the fly model suggest a possible conservation of the role of human OATPs in steroid depletion in cancer-induced cachexia.

## Discussion

The *Drosophila* larva has recently emerged as a genetic model to study several aspects of normal physiology. Here we use this model to study cachexia, a pathophysiological condition linked to tumor development.

The prevalence of cachexia is dramatically increased in the larval population when *Ecl* or *Oatp33Eb*, two members of the *Oatp* transporters, are upregulated in tumors. However, their up-regulation in non-tumorous discs is not sufficient to promote a catabolic conversion. This suggests that additional pro-

cachectic, tumor-derived factors are required to promote the cachectic state, as recently established using the adult *Drosophila* model. Indeed, we found that forcing expression of these two Oatps is sufficient to promote cachexia in the non-cachectic *rn>avl<sup>RNAi</sup>* tumor model. Among the previously described pro-cachectic factors, Imp-L2 is found upregulated in our cachectic tumor model. However, its knockdown in the tumors does not reduce the prevalence of cachexia, suggesting that Imp-L2 does not play a major role in triggering cachexia in our model. Neither Pvf1, nor branchless (*bnl*), two cachectic factors identified in *Drosophila* are upregulated in tumors in our conditions (see Suppl. Fig. 3B, Suppl. Fig. 6K), suggesting that other unidentified factors could contribute to cachexia in this model.

Our finding that cachectic tumor-bearing animals have reduced levels of the steroid Ec parallels the prevalence of hypogonadism in men with cancer cachexia (Burney *et al.*, 2012). Remarkably, the capacity of cachectic animals to produce Ec or to convert it into the active form 20-E seems unaffected and this reduction mostly results from an increase in steroid uptake by the tumor. In addition, we observed that upregulating intra-tumoral EcR signaling was not sufficient to promote cachexia, indicating that the reduction of circulating ecdysone levels is key for this process.

Interestingly, the gene encoding Oatp74D, recently described as Ecdysone Importer (Eci), is not induced in cachectic tumors and its silencing does not reduce the prevalence of cachexia. Rather, we find that another member of the Oatp family, Oatp33Eb, is specifically induced in our model of cachectic tumors. The link between this Oatp member and ecdysone import is not molecularly established. However, we find that silencing Oatp33Eb efficiently rescues both cachexia and the levels of circulating ecdysone, while its over-expression induces cachexia and EcR signaling in the tumor and reduces circulating ecdysteroid levels. This transporter is not highly expressed in normally developing imaginal discs, indicating a specific upregulation in a tumor context. We have no mechanistic explanation for such upregulation, but we observed that *Oatp33Eb* upregulation is associated with *dlg* loss-of-function, but not *Ras<sup>V12</sup>* overexpression, suggesting a possible link with a loss of cell polarity. Moreover, silencing EcR in tumors prevents upregulation of *Oatp33Eb*, suggesting that EcR signaling exerts a positive feedback on its expression, in line with numerous EcR/Usp binding sites found in the *oatp33Eb* promoter. This could explain the efficient rescue of cachexia observed when EcR signaling is inhibited in tumors (*tumor>EcR<sup>DN</sup>*). Interestingly, growing *tumor>EcR<sup>DN</sup>* animals on *erg2Δ* food was sufficient to induce cachexia in all larvae, confirming that reducing circulating levels of ecdysone is the limiting trigger for cachectic conversion. A similar feedback mechanism has been described in the case of the vertebrate *Oatp1* gene, whose expression is controlled by the level of androgen in the kidney (Isern *et al.*, 2001).

The role of human Oatps in transporting xenobiotics has made them possible markers for chemotherapy disposition (Schulte and Ho, 2019). Several evidences in cell and tumor models also indicate a possible role for OATP1B3 (the closest vertebrate homolog of the fly Oatp33Eb) in transporting steroid hormones

(Hamada *et al.*, 2008). Some of these transporters are highly expressed in tumors associated with high prevalence of cachexia including breast, colon, prostate, pancreatic and head & neck cancers, with little expression in normal tissues. This mimics the situation observed with Oatp33Eb in our tumor model and suggests that OATPs could serve as biomarkers or therapeutic targets for the early stages of cancer-induced cachexia.

### **Limitations of the study**

In this study, tumor-induced Oatp33Eb was shown to play a key role in promoting cachexia in larval peripheral tissues. The mechanisms underlying Oatp33Eb transcriptional regulation and downstream signaling should be explored in the future, as well as the possible role of OATPs in mammals as therapeutic targets in cachectic tumors.

### **Acknowledgements**

We thank Mike O'Connor, and lab members for insightful discussions and comments on the manuscript. We thank Wenjie Sun for bioinformatic analysis of SLCO genes. We thank the Vienna Drosophila RNAi Center and the Bloomington stock center for lines. We thank the PICT-IBiSA@BDD light-microscopy facility of Institut Curie. This work was supported by Institut Curie, CNRS, INSERM, ARC Fondation (grant n° PDF20180507272 to P.S.), FRM, European Research Council (Advanced Grant n°694677 to P.L.) and the Labex DEEP program (ANR-11-LABX-0044, ANR-10-IDEX-0001-02).

### **Author contributions**

Conceptualization, P.L. and P.S., Methodology, P.L. and P.S., Investigation, P.S., Writing and editing, P.L. and P.S., Funding Acquisition, P.L. and P.S.; Supervision, P.L.

### **Declaration of interests**

The authors declare no competing interests.

### **References**

- Bennani-Baiti, N. and Walsh, D. (2011) 'Animal models of the cancer anorexia-cachexia syndrome.', *Supportive care in cancer : official journal of the Multinational Association of Supportive Care in Cancer*, 19(9), pp. 1451–63. doi: 10.1007/s00520-010-0972-0.
- Bjordan, M. *et al.* (2014) 'Sensing of amino acids in a dopaminergic circuitry promotes rejection of an incomplete diet in drosophila', *Cell*, 156(3), pp. 510–521. doi: 10.1016/j.cell.2013.12.024.
- Britton, J. S. *et al.* (2002) 'Drosophila's insulin/PI3-kinase pathway coordinates cellular metabolism with nutritional conditions', *Developmental Cell*. *Dev Cell*, 2(2), pp. 239–249. doi: 10.1016/S1534-

5807(02)00117-X.

Brumby, A. M. and Richardson, H. E. (2005) 'Using *Drosophila melanogaster* to map human cancer pathways', *Nature Reviews Cancer*. Nat Rev Cancer, pp. 626–639. doi: 10.1038/nrc1671.

Burney, B. O. *et al.* (2012) 'Low testosterone levels and increased inflammatory markers in patients with cancer and relationship with cachexia', *Journal of Clinical Endocrinology and Metabolism*. J Clin Endocrinol Metab, 97(5). doi: 10.1210/jc.2011-2387.

Cherbas, L. *et al.* (2003) 'EcR isoforms in *Drosophila*: Testing tissue-specific requirements by targeted blockade and rescue', *Development*. Development, pp. 271–284. doi: 10.1242/dev.00205.

Devorkin, L. and Gorski, S. M. (2014) 'Lysotracker staining to aid in monitoring autophagy in *Drosophila*', *Cold Spring Harbor Protocols*. Cold Spring Harbor Laboratory Press, 2014(9), pp. 951–958. doi: 10.1101/pdb.prot080325.

Droujinine, I. A. and Perrimon, N. (2016) 'Interorgan Communication Pathways in Physiology: Focus on *Drosophila*', *Annual Review of Genetics*, 50(1), pp. 539–570. doi: 10.1146/annurev-genet-121415-122024.

Fearon, K., Arends, J. and Baracos, V. (2013) 'Understanding the mechanisms and treatment options in cancer cachexia.', *Nature reviews. Clinical oncology*, 10(2), pp. 90–9. doi: 10.1038/nrclinonc.2012.209.

Figuroa-Clarevega, A. and Bilder, D. (2015) 'Malignant *Drosophila* tumors interrupt insulin signaling to induce cachexia-like wasting.', *Developmental cell*, 33(1), pp. 47–55. doi: 10.1016/j.devcel.2015.03.001.

Folk, D. G., Han, C. and Bradley, T. J. (2001) 'Water acquisition and partitioning in *Drosophila melanogaster*: Effects of selection for desiccation-resistance', *Journal of Experimental Biology*. J Exp Biol, 204(19), pp. 3323–3331. Available at: <https://pubmed-ncbi-nlm-nih-gov.proxy.insermbiblio.inist.fr/11606606/> (Accessed: 9 September 2020).

Hamada, A. *et al.* (2008) 'Effect of SLC01B3 haplotype on testosterone transport and clinical outcome in caucasian patients with androgen-Independent prostatic cancer', *Clinical Cancer Research*. Clin Cancer Res, 14(11), pp. 3312–3318. doi: 10.1158/1078-0432.CCR-07-4118.

Honors, M. A. and Kinzig, K. P. (2012) 'The role of insulin resistance in the development of muscle wasting during cancer cachexia', *Journal of Cachexia, Sarcopenia and Muscle*. Wiley Online Library, pp. 5–11. doi: 10.1007/s13539-011-0051-5.

Isern, J. *et al.* (2001) 'Functional analysis and androgen-regulated expression of mouse organic anion transporting polypeptide 1 (Oatp1) in the kidney', *Biochimica et Biophysica Acta - Gene Structure and Expression*. Biochim Biophys Acta, 1518(1–2), pp. 73–78. doi: 10.1016/S0167-4781(01)00169-5.

Katsuyama, T. and Paro, R. (2013) 'Innate immune cells are dispensable for regenerative growth of imaginal discs', *Mechanisms of Development*. Mech Dev, 130(2–3), pp. 112–121. doi: 10.1016/j.mod.2012.11.005.

Kimura, S. *et al.* (2008) '*Drosophila* arginine methyltransferase 1 (DART1) is an ecdysone receptor co-

repressor', *Biochemical and Biophysical Research Communications*. Academic Press, 371(4), pp. 889–893. doi: 10.1016/j.bbrc.2008.05.003.

Kwon, Y. *et al.* (2015) 'Systemic organ wasting induced by localized expression of the secreted insulin/IGF antagonist ImpL2.', *Developmental Cell*, 33(1), pp. 36–46. doi: 10.1016/j.devcel.2015.02.012.

Leopold, P. and Perrimon, N. (2007) 'Drosophila and the genetics of the internal milieu.', *Nature*, 450(7167), pp. 186–8. doi: 10.1038/nature06286.

Molfinio, A. *et al.* (2019) 'Investigational drugs for the treatment of cancer cachexia: a focus on phase I and phase II clinical trials', *Expert Opinion on Investigational Drugs*. Taylor and Francis Ltd, 28(8), pp. 733–740. doi: 10.1080/13543784.2019.1646727.

Obaidat, A., Roth, M. and Hagenbuch, B. (2012) 'The Expression and Function of Organic Anion Transporting Polypeptides in Normal Tissues and in Cancer', *Annual Review of Pharmacology and Toxicology*. Annual Reviews, 52(1), pp. 135–151. doi: 10.1146/annurev-pharmtox-010510-100556.

Okamoto, N. *et al.* (2018a) 'A Membrane Transporter Is Required for Steroid Hormone Uptake in Drosophila', *Developmental Cell*. Cell Press, 47(3), pp. 294-305.e7. doi: 10.1016/j.devcel.2018.09.012.

Okamoto, N. *et al.* (2018b) 'A Membrane Transporter Is Required for Steroid Hormone Uptake in Drosophila', *Developmental Cell*. Cell Press, 47(3), pp. 294-305.e7. doi: 10.1016/j.devcel.2018.09.012.

Pagliarini, R. A. and Xu, T. (2003) 'A Genetic Screen in Drosophila for Metastatic Behavior', *Science*, 302(5648), pp. 1227–1231. doi: 10.1126/science.1088474.

Petryk, A. *et al.* (2003) 'Shade is the Drosophila P450 enzyme that mediates the hydroxylation of ecdysone to the steroid insect molting hormone 20-hydroxyecdysone', *Proceedings of the National Academy of Sciences of the United States of America*. Proc Natl Acad Sci U S A, 100(SUPPL. 2), pp. 13773–13778. doi: 10.1073/pnas.2336088100.

Rewitz, K. F., Yamanaka, N. and O'Connor, M. B. (2010a) 'Steroid Hormone Inactivation Is Required during the Juvenile-Adult Transition in Drosophila', *Developmental Cell*. NIH Public Access, 19(6), pp. 895–902. doi: 10.1016/j.devcel.2010.10.021.

Rewitz, K. F., Yamanaka, N. and O'Connor, M. B. (2010b) 'Steroid Hormone Inactivation Is Required during the Juvenile-Adult Transition in Drosophila', *Developmental Cell*. Dev Cell, 19(6), pp. 895–902. doi: 10.1016/j.devcel.2010.10.021.

Schulte, R. R. and Ho, R. H. (2019) 'Organic anion transporting polypeptides: Emerging roles in cancer pharmacology', *Molecular Pharmacology*. American Society for Pharmacology and Experimental Therapy, pp. 490–506. doi: 10.1124/mol.118.114314.

Song, W. *et al.* (2019) 'Tumor-Derived Ligands Trigger Tumor Growth and Host Wasting via Differential MEK Activation', *Developmental Cell*. Cell Press, 48(2), pp. 277-286.e6. doi: 10.1016/j.devcel.2018.12.003.

Sonoshita, M. and Cagan, R. L. (2017) 'Modeling Human Cancers in Drosophila.', *Current topics in*

*developmental biology*, 121, pp. 287–309. doi: 10.1016/bs.ctdb.2016.07.008.

Yamanaka, N., Rewitz, K. F. and O'Connor, M. B. (2013) 'Ecdysone control of developmental transitions: Lessons from drosophila research', *Annual Review of Entomology*. Annu Rev Entomol, pp. 497–516. doi: 10.1146/annurev-ento-120811-153608.

## Figure legends

### Figure 1. Tumor-induced cachexia triggers hormonal imbalance in *Drosophila* larvae.

(A,B) Representative images of control and tumor-bearing larvae showing bloating (A) and percentage of bloating animals with the indicated genotypes (n=200 for each genotype). Only *tumors>+* and *tumors>Ecl*-larvae showed bloating (27% and 85%, respectively). \*\*\*p<0,001.

(C) Quantification of larval volumes with the indicated genotypes (n=50 for each genotype). \*\*p<0,05, \*\*\*p<0,001.

(D) Differences in dry mass (calculated with the formula dry mass\*100/wet mass) in larvae with the indicated genotypes (n=50 for each genotype). In each column, the delta between *CTRL* and tumor conditions is plotted. Bloating *tumor>* and *tumors>Ecl* larvae show significant dry weight loss. \*\*p<0,05, \*\*\*p<0,001.

(E) Peripheral tissue wasting in tumor-bearing larvae. LysoTracker labels acidic vesicles (purple) and Nile Red labels lipid droplets (red) in fat body cells from larvae with the indicated genotypes.  $\alpha$ Actinin (white) and Phalloidin (green) staining show larval muscle morphology. The dotted line surrounds a GFP positive cell in *tumors>shd<sup>RNAi</sup>*.

(F) Tumor size in larvae with the indicated genotypes (n=30 per genotype). The dotted line represents the mean. \*p<0,05.

(G) Differences in food intake measured using blue dye Erioglaucine in the food (n=12 groups of 8 larvae each). Values relative to tumor-less controls are showed, \*p<0,05.

(H) Insulin sensitivity in fat body cells by measuring the delta in membrane *tGPH* in fat bodies incubated with or without insulin. The delta for Ctrl and various tumor conditions is plotted. \*\*\*p<0,001. See Suppl. Fig. 1F for confocal images.

(I, J) Concentration of hemolymph glucose (I) and trehalose (J) from larvae with the indicated genotypes (mean +/- SEM, \*\*\*p<0,001). The plotted values correspond to the mean.

See also Figure S1, S2, S3.

### Figure 2. Ecdysone uptake by the tumor causes a decrease in ecdysone signaling in healthy tissues.

(A, D) Tumors cachectic and non-cachectic stained with  $\alpha$ -EcR,  $\alpha$ -Broad and carrying the EcRE\_LacZ reporter stained with  $\alpha$ - $\beta$ -Gal (A), together with a quantification of the pixel intensity (B-D).

(E) mRNA levels of Ec targets in cachectic tumors versus non-cachectic from larvae with the same genotype, measured by RT-PCR. The results shown are mean +/- SEM. \*p<0,05, \*\*\*p<0,001.

(F) Quantification by measuring the delta of circulating 20-E (/ul hemolymph/larva) found in the hemolymph of larvae with the indicated genotypes. \*\*\*p<0,001.

(G-J) Fat bodies from larvae with the indicated genotype carrying the EcREGFP reporter stained with  $\alpha$ -GFP (G, in green) and stained with  $\alpha$ -EcR (I, in white) and quantifications of the pixel intensities (H, J). The dotted line represents the mean. \*p<0,05, \*\*\*p<0,001.

(K) mRNA levels of ecdysone targets (*broad*, *E74A*, *E78* and *DHR3*) in fat bodies from different genotypes, measured by RT-PCR. The results shown are mean +/- SEM. \*p<0,05, \*\*p<0,01.

### **Figure 3. Cachexia inversely correlates with the levels of circulating Ecdysone.**

(A-D) The cachectic phenotype is rescued by the addition of 20-E. Percentage of animals with bloating defects (A, n=200 for each genotype), mean larval volume (B, n=50 for each genotype), water volume (C, n=50 for each genotype), and extractable hemolymph (D, n=50 for each genotype) from larvae reared on standard food versus food containing exogenous 20-E, with the indicated genotypes. The dotted line represents the mean. \*\*p<0,01, \*\*\*p<0,001.

(E,F) Tumor sizes (E, n=30 per genotype) and metastasis (F, n=200 for each genotype) in larvae reared on standard food versus food containing 20-E. In F, the dotted line represents the mean, no significant differences were found.

(G) Differences in the content of dry mass observed in larvae with the indicated genotypes fed with standard vs 20-E-food (n=50 for each genotype). The delta between CTRL and tumor-bearing animals is plotted as a single value. \*\*\*p<0,001.

(H-K) The cachectic phenotype is aggravated on *erg2Δ* yeast-containing food. Percentage of animals with bloating defects (H, n=40 for each genotype), larval volume (I, n=40 for each genotype), water volume (J, n=40 for each genotype) and of volumes of extractable hemolymph (K, n=40 for each genotype) from larvae reared on standard food versus food made from *erg2Δ* yeast. The dotted line represents the mean. \*\*p<0,01, \*\*\*p<0,001.

(L) Magnified larvae reared in food containing the *erg2* mutant yeast strain *erg2Δ*. All larvae-bearing tumors showed swelling defects independently of their genetic background.

(M,N) Tumor sizes (M, n=30 per genotype) and aggressiveness (N, n=40 for each genotype) in larvae with the indicated genotypes reared on standard food versus food containing *erg2Δ* yeast. The dotted line represents the mean. \*p<0,05, \*\*p<0,01.

(O) Differences in dry mass observed in larvae with the indicated genotypes fed with standard or *erg2Δ*-food (n=40 for each genotype). The delta between *CTRL*> and *tumor*> is plotted as a single value. \*\*\*p<0,001.

See also Figure S4, S5.

**Figure 4. The OATP transporter *Oatp33Eb* is upregulated in the tumor and drives the sink effect (I).**

(A) mRNA levels of *Drosophila Oatp* genes from CTRL and tumorous discs measured by RT-PCR. Shown results are mean +/- SEM. \*\*\* $p < 0,001$ .

(B, C) Percentage of larvae with bloating defects after the individual inhibition of each *Oatp* gene with an RNAi line (B,  $n=200$  for each genotype) and metastasis (C,  $n=200$  for each genotype).

(D) Tumor sizes in larvae after the individual inhibition of each *Oatp* gene with an RNAi line ( $n=30$  per genotype). The dotted line represents the mean. \* $p < 0,05$ .

(E, F) Water volume (E,  $n=50$  for each genotype) and volumes of extractable hemolymph (F,  $n=50$  for each genotype). The quantity of hemolymph is restored after *Oatp33Eb* inhibition in the tumor. The dotted line represents the mean. \* $p < 0,05$ , \*\*\* $p < 0,001$ .

(G) Food intake of larvae with the indicated genotypes ( $n=11$  groups of 8 larvae each one). Values are shown relative to control, \* $p < 0,05$ .

(H) Differences in dry mass ( $n=50$  for each genotype) in larvae with the indicated genotype. \*\* $p < 0,01$ , \*\*\* $p < 0,001$ .

(I) Fat bodies and muscles from tumors, *tumors>Oatp33Eb<sup>RNAi</sup>* and *tumors>Oatp33Eb* animals. Lipid droplets are shown in red, Glucose uptake in yellow, acidic vesicles in purple and muscle fibers in white.

(J) *Oatp33Eb* expression in different tumors measured by RT-PCR (mean +/-SEM). \*\*\* $p < 0,001$ .

(K) The protein *Oatp33Eb* localizes at the cell membrane. Tumors overexpressing the *Oatp33Eb-Flag-HA* stained with  $\alpha$ -Flag (yellow), DAPI (white) and GFP to label cancer cells. The grey square shows a magnification of a transversal section of the tumor.

See also Figure S6.

**Figure 5. The SLCO transporter *Oatp33Eb* is upregulated in the tumor and drives the sink effect (II).**

(A, C) Tumors from larvae with the indicated genotype stained with  $\alpha$ -EcR and  $\alpha$ -Broad (A) and quantifications of the pixel intensity (B-C).

(D, E) EcR staining (D) and quantification (E) in fat body cells from tumors, *tumors>Oatp33Eb<sup>RNAi</sup>* and *tumors>Oatp33Eb* animals. EcR is significantly reduced in *tumors>* and *tumors>Oatp33Eb* but not *tumors>Oatp33Eb<sup>RNAi</sup>* fat bodies. The dotted line represents the mean. \* $p < 0,05$ .

(F) mRNA levels of ecdysone targets (*broad* and *E78*) measured by RT-PCR in the fat body of animals with the indicated genotypes. The results shown are mean +/- SEM. \* $p < 0,05$ .

(G) Quantification by measuring the delta of circulating 20-E ( $\mu$ l hemolymph/larva) found in the hemolymph of larvae with the indicated genotypes.

(H) Representative images of control and tumor-bearing larvae showing bloating with the indicated genotypes.

(I, J, K) Differences in water volume, extractable hemolymph and dry mass (n=50 for each genotype) from larvae with the indicated genotypes. The dotted line represents the mean. \*\*p<0,01, \*\*\*p<0,001.

(L, M) Representative images (L) and percentage of bloating adult females after tumor injection with the indicated genotypes (M).

(N) Survival curve of adult females after tumor injection with the indicated genotypes. Lifespan was significantly longer in *tumor>Oatp33Eb<sup>RNAi</sup>* and *PBS-injected* flies than in *tumor>injected* flies. \*p<0,05, \*\*\*p<0,001.

See also Figure S7, S8.

## STAR METHODS

### KEY RESOURCES TABLE

REAGENT or RESOURCE	SOURCE	IDENTIFIER
<b>Antibodies</b>		
$\alpha$ -GFP	Abcam	ab13970
$\alpha$ -actinin	DSHB	2G3-3D7
Phalloidin-FITC	Sigma-Aldrich	P-5282
$\alpha$ -EcR	DSHB	Ag10.2
$\alpha$ -Serotonin	Sigma-Aldrich	S5545
$\alpha$ -Ptth	Our laboratory	-
$\alpha$ -Broad	DSHB	25E9.D7
$\alpha$ - $\beta$ -Gal	Promega	Z378B
$\alpha$ -Flag	Sigma-Aldrich	F1804
<b>Chemicals, peptides and recombinant proteins</b>		
Lysotracker Red	Invitrogen	DND-99
Nile Red	Merck	N3013
2-NBDG	Invitrogen	N13195
Erioglucine disodium salt	Merck	861146
Slowfade <sup>TM</sup> Diamond	Thermofisher	S36967
Prolong <sup>TM</sup>	Thermofisher	P36984
20-Hydroxyecdysone	Merck	H5142
Human insulin	Sigma-Aldrich	I9278
<b>Critical commercial kits</b>		
RNeasy <sup>®</sup> Lipid Tissue Mini kit	Qiagen	74804
RNeasy <sup>®</sup> Plus Micro kit	Qiagen	74034
DNAse I	Biolabs	M0303S
SuperScript II reverse transcriptase	Invitrogen	18064022
Power SYBR <sup>TM</sup> Green PCR Master Mix	Applied Biosystems	4367659
20-Hydroxyecdysone detection kit	Bertin reagents	A05120
Porcine Trehalase	Merck	T8778-1UN
GAGO-20	Merck	

NEBuilder® HiFi DNA Assembly Cloning Kit	Biolabs	E5520S
Experimental models: Organisms/strains		
<i>w<sup>118</sup></i>	BDSC	3605
<i>eyFLP, act&gt;FRT-y<sup>+</sup>-FRT&gt;Gal4, UAS-GFP, UAS-Ras<sup>v12</sup>, UAS-dlg<sup>RNAi</sup></i>	From J.Cordero's lab	-
<i>EcRE_LacZ</i>	BDSC	4517
<i>nub-Gal4</i>	BDSC	86108
<i>rn-Gal4</i>	BDSC	7405
<i>pdm2-Gal4</i>	BDSC	75571
<i>UAS-yki<sup>SA</sup></i>	BDSC	28818
<i>elav.Gal80</i>	BDSC	98193
<i>syb.Gal80</i>	BDSC	79028
<i>dlg<sup>40.2</sup></i>	From J.Cordero's lab	-
<i>UAS-Ecl</i>	Okamoto et al., 2018b	-
<i>UAS-EcR<sup>DN</sup></i>	Cherbas et al., 2003	-
<i>UAS-shd<sup>RNAi</sup></i>	BDSC	67356
<i>UAS-Cyp18a1</i>	Rewitz, Yamanaka and O'Connor, 2010a	
<i>tGPH</i>	Britton <i>et al.</i> , 2002	-
<i>EcRE_GFP</i>	Kimura <i>et al.</i> , 2008	-
<i>UAS-Cyp18a1<sup>RNAi</sup></i>	VDRC	104180
<i>UAS-avl<sup>RNAi</sup></i>	VDRC	5413
<i>UAS-Ecl<sup>RNAi</sup></i>	VDRC	37295
<i>UAS-Oatp26F<sup>RNAi</sup></i>	VDRC	2650
<i>UAS-Oatp30B<sup>RNAi</sup></i>	VDRC	22983
<i>UAS-Oatp33Ea<sup>RNAi</sup></i>	VDRC	45896
<i>UAS-Oatp33Eb<sup>RNAi</sup></i>	VDRC	100431
<i>UAS-Oatp58Da<sup>RNAi</sup></i>	VDRC	6623
<i>UAS-Oatp58Db<sup>RNAi</sup></i>	VDRC	100348
<i>UAS-Oatp58Dc<sup>RNAi</sup></i>	VDRC	39469
Oligonucleotides		
rp49 FW: AAGAAGCGCACCAAGCACTTCATC	Colombani et al., 2005	-
rp49 RV: TCTGTTGTCGATACCTTGGGCTT	Colombani et al., 2005	-
Ecl FW: TGCAGTGCCGCTCTCAACTGTACC	Okamoto et al., 2018b	-
Ecl RV: TCACAGTAACCGTTGACCGCCTCC	Okamoto et al., 2018b	-
EcR FW: ACCAGCGTTTACAAAGATACCC	Boulan et al., 2020	-
EcR RV: CATCATCACCTCCGACGAG	Boulan et al., 2020	-
dilp8 FW: CGACAGAAGGTCCATCGAGT	Colombani et al., 2009	-
dilp8 RV: GTTTTGCCGGATCCAAGTC	Colombani et al., 2009	-
E74A FW: TGAGACGCGAGGAATACCCTGGAC	Boulan et al., 2020	-
E74A RV: AACTGCCAGCGTGTAGCCGTTTCC	Boulan et al., 2020	-
E78 FW: CATGTGGCCCGTTGATC	Boulan et al., 2020	-
E78 RV: CGTTGACAAAGTCAGAATCGTAGAG	Boulan et al., 2020	-
DHR3 FW: AATATTGTAGACTGCAAAAGTGCCTA	Boulan et al., 2020	-
DHR3 RV: GGACATCCTGCCGAACCTTA	Boulan et al., 2020	-
DHR4 FW: TGCTCTCCACATACCAGAGA	Boulan et al., 2020	-
DHR4 RV: CACGAAGGGCACATAGAACA	Boulan et al., 2020	-
ftz-F1 FW: TTGCCGCTTTTTAAGAACATTT	Boulan et al., 2020	-
ftz-F1 RV: TGACATTTAATCTCTCCAGGAGTATC	Boulan et al., 2020	-
broad FW: TCTGTGACTCGGTGACATTTGCCGA	Boulan et al., 2020	-

broad RV: TTACTAGACCGCTTGCCGGATTGT	Boulan et al., 2020	-
impl2 FW: AAGAGCCGTGGACCTGGTA	Song et al., 2018	-
impl2 RV: TTGGTGAACCTGAGCCAGTCG	Song et al., 2018	-
shd FW: GCACGAGGTATATGCGGATT	Hackney et al., 2012	-
shd RV: GGAGGTCGGAATGGGTATTT	Hackney et al., 2012	-
tai FW: CTCCGTTTGGCTCTAACTCG	Colombani et al., 2005	-
tai RV: TGTTGTTGCAGCGTTCTACC	Colombani et al., 2005	-
usp FW: CCTGTGCCAAGTGGTCAACAAACA	Hackney et al., 2012	-
usp RV: ATCCAAGCGGCTTTCAGCAGAATC	Hackney et al., 2012	-
4E-BP FW: CCGGCGGAACCCTCTACT	Colombani et al., 2005	-
4E-BP RV: GGGAGCCACGGAGATTCTTC	Colombani et al., 2005	-
oatp26F FW: TCAACTCAGCCTGACCAGCGACAG	Okamoto et al., 2018b	-
oatp26F RV: ATGGGCAAGGCGATGAGCAGACAC	Okamoto et al., 2018b	-
oatp30b FW: GAGGAGGACTTCGATGAGGAGCAG	Okamoto et al., 2018b	-
oatp30b RV: ATCATCACCAGCAGCGAGAGCAGC	Okamoto et al., 2018b	-
oatp33Ea FW: ATCTACGGAGCTGGTCACGAGGTG	Okamoto et al., 2018b	-
oatp33Ea RV: TTGTCCACTCCACAGAGTCGCTCG	Okamoto et al., 2018b	-
oatp33Eb FW: TTGCGTTGGCTTTCGCTACTGGG	Okamoto et al., 2018b	-
oatp33Eb RV: TGGAGGGAATCACAGCCACCACAC	Okamoto et al., 2018b	-
oatp58Da FW: TTGAGACATGACAGAGGAGCGAGG	Okamoto et al., 2018b	-
oatp58Da RV: TGGCAAATCTTTCGATGGAGGGGC	Okamoto et al., 2018b	-
oatp58Db FW: CTACGCTAGTCGAGGACATCGTCC	Okamoto et al., 2018b	-
oatp58Db RV: TGTCAGCCGCAAAGCTTCTTCGCC	Okamoto et al., 2018b	-
oatp58Dc FW: AGAGCGAGAATCCCAGTAGCCTGG	Okamoto et al., 2018b	-
oatp58Dc RV: TTCGGAGTGGTCTCTTCACCGTC	Okamoto et al., 2018b	-
ptth FW: CACAGAGATGGCGATGGTC	Colombani et al., 2005	-
ptth RV: AGATCCACGAGCTCATTCTG	Colombani et al., 2005	-
nvd FW: AGCAACTTGTGTGTCATGCTTGGG	Hackney et al., 2016	-
nvd RV: TTGGCTCCTAGGTGAGGGCAATAA	Hackney et al., 2016	-
spok FW: GCTCTTGGCGGTGATCGAAACAA	Hackney et al., 2016	-
spok RV: CGCCGAGCTAAATTTCTCCGCTTT	Hackney et al., 2016	-
dib FW: ATGGTGGTGCCATTGATATGC	Colombani et al., 2005	-
dib RV: GACGAGCTCCAAAGGTAAGCA	Colombani et al., 2005	-
phm FW: TCGTCGTGGGCGATTATTTTA	Ignesti et al., 2018	-
phm RV: AAGGCCACTGGTCCATGT	Ignesti et al., 2018	-
sad FW: CAACGGGGACTGTTCTTCAT	Hackney et al., 2016	-
sad RV: CAGTGCGTCTTTTCCACTGA	Hackney et al., 2016	-
ecd FW: AGCGACTCGGATGAGTGGTTGAAT	Hackney et al., 2016	-
ecd RV: GGCATTCATTTGTCCGTTCCGCTT	Hackney et al., 2016	-
dare FW: ATCTAGTTGCGTGGATACGGGCAT	Hackney et al., 2016	-
dare RV: AGCCAGCCAGCTACATAAAGTCCA	Hackney et al., 2016	-
mld FW: ACTGTGCGAACGGAATTGAACAGC	Hackney et al., 2016	-
mld RV: TGAGGATGCCATTGAGTGTGGTCT	Hackney et al., 2016	-
wok FW: ATCCCTGCTTCTCCGCTTTAAGT	Hackney et al., 2016	-
wok RV: AGAAGACCTTCGGTGACTGCTGTT	Hackney et al., 2016	-
pvf1 FW: CTGTCCGTGTCCGCTGAG	Song et al., 2018	-
pvf1 RV: CTCGCCGGACACATCGTAG	Song et al., 2018	-
bnl FW: CTCAAGTCCGAGGCCAAG	Newton et al., 2020	-
bnl RV: GGATGGCTCTTTTTCGGAGCA	Newton et al., 2020	-
<b>Primers for UAS-Oatp33Eb cloning: pUAST-attB_FW</b>	This study	-

AAAAAAAAAAAAAGAATTCGTTAACAGATCTGC		
<b>Primers for UAS-Oatp33Eb cloning:</b> pUAST-attB_RV CGGGAGCAAACCTCCAATTCCTATTTCAGAG	This study	-
<b>Primers for UAS-Oatp33Eb cloning:</b> Oatp33Eb_FW AATAGGGAATTGGAGTTTGCTCCCGTTCCTC	This study	-
<b>Primers for UAS-Oatp33Eb cloning:</b> Oatp33Eb_RV TGTTAACGAATTCCTTTTTTTTTTTTTTTGCTTTTAAATGA AATGAAG	This study	-
Recombinant DNA		
<i>pUASattB-Oatp33Eb</i>	This study	-
<i>pUASattB-Oatp33Eb-FLAH-HA</i>	BDGP	UFO06268
Software and algorithms		
GraphPad Prism V8	GraphPad Software	<a href="https://www.graphpad.com/scientificsoftware/prism/">https://www.graphpad.com/scientificsoftware/prism/</a>
Excel	Microsoft	
Jaspar database	Online tool	<a href="http://jaspar2016.genereg.net/">http://jaspar2016.genereg.net/</a>
Photoshop	Adobe	-
ImageJ	NIH	

## RESOURCE AVAILABILITY

### Lead contact

Further information and requests for resources and reagents should be directed to and will be fulfilled by the lead contact, Pierre Léopold ([pierre.leopold@curie.fr](mailto:pierre.leopold@curie.fr)).

### Material availability

All plasmids and fly lines generated in this study are available upon request to the Lead contact (see above).

### Data and code availability

This study did not generate data sets or codes.

## EXPERIMENTAL MODEL AND SUBJECT DETAILS

### *Drosophila* strains and maintenance

Flies were reared and experiments were performed on fly food containing, per liter: 50g yeast powder, 35g wheat flour, 7.5 g agar, 55g sugar, 25ml Methyl and 4ml propionic acid. Experiments were done at 25°C. For all experiments, both males and females were used. For all experiments, a precise staging of the animals was done with 4-hours egg laying collected on agar plates with yeast. The next day, recently hatched L1 larvae were collected 24 hours AEL and reared in tubes (forty larvae each) containing

standard food. The developmental stage or time of development at which analysis were done is indicated in the methods section. *Drosophila* strains used in this study and their origin are in the KRT.

## METHOD DETAILS

**Generation of transgenic flies.** To generate the *UAS-Oatp33Eb* and *UAS-Oatp33Eb-FLAH-HA* fly lines, the *pUASattB-Oatp33Eb* and *pUASattB-Oatp33Eb-FLAH-HA* constructs were introduced into the germ line by injections in the presence of the *PhiC31* integrase and inserted in the *attP2*-landing site on the 3R chromosome (BDSC 8622, BestGene). *Oatp33Eb* coding sequence was PCR amplified from the BDGP clone RE09129 (full cDNA *Oatp33Eb* into pFLC-1 vector) and cloned into the *pUAST-attB* vector using the following primers with homology sequences between insert and vector:

AAAAAAAAAAAAAGAATTCGTTAACAGATCTGC (pUAST-attB\_FW), CGGGAGCAAACCTCCAATTCCTATTCAGAG (pUAST-attB\_RV), AATAGGGAATTGGAGTTTGCTCCCGTTCCTC (Oatp33Eb\_FW) and TGTTAACGAATTCTTTTTTTTTTTTTTTTGGCTTTTAAATGAAATGAAG (Oatp33Eb\_RV). For the cloning, the standard protocol of the Cloning Kit NEBuilder was performed.

For the *UAS-Oatp33Eb-FLAH-HA*, the BDGP Clone UFO06268 (full cDNA *Oatp33Eb-RA* into a *pUAST-CFLAGHA-BD-PHI*) was already available at the *Drosophila* Studies Hybridoma Bank (DSHB).

**Tumor generation.** We induced the formation of metastatic tumors in *Drosophila* larvae as described in Pagliarini and Xu, 2003. We utilized *eyeless* promoter-driven FLP recombinase expression (*eyFLP*) to activate the *act>y+>Gal4* construct. This allowed the expression of the oncogenic *ras*<sup>V12</sup> mutant with an interference RNA to inhibit the tumor suppressor gene *disc large* (*dlg*<sup>RNAi</sup>) into GFP-labeled cells specifically in the developing larval eye-antennal imaginal discs, which altogether is known to induce cachexia in *Drosophila* adults after transplantation (Figuroa-Clavevega and Bilder, 2015; Kwon *et al.*, 2015). Females containing *eyFLP; UAS-Ras*<sup>V12</sup>, *UAS-dlg*<sup>RNAi</sup>/*CyO*<sub>Gal80</sub><sup>TS</sup>; *act>y+>Gal4*, *UAS-GFP/TM6B* were crossed with the desired males. For each genotype, we used as a control larvae from the same vial but tumor-free (*eyFLP; +/CyO*<sub>Gal80</sub><sup>TS</sup>; *act>y+>Gal4*, *UAS-GFP/+*). Tumor size was analyzed at 120h AEL with Fiji software. The number of metastasis was counted under a GFP scope. Tumor injection into the abdomen of *Drosophila* adults was conducted as in Figuroa-Claveraga *et al.*, 2015. Survival was calculated using the Kaplan-Meier method and compared statistically using the log rank test.

**Modulation of ecdysone signaling.** We used distinct tools to modify ecdysone signaling in peripheral tissues. EcR<sup>DN</sup> is a dominant negative form of EcR, which binds to the promoter region of target genes but is deficient for transcriptional activation (Cherbas *et al.*, 2003). The *shade* (*shd*)-RNAi construct blocks expression of *shade*, a gene coding for a P450 enzyme that converts ecdysone in its active form 20-hydroxyecdysone (Petryk *et al.*, 2003). The *Cyp18a1* gene codes for an enzyme that degrades ecdysone

(Rewitz, Yamanaka and O'Connor, 2010a). Ecl is an Oatp importer (Oatp74D) that transports ecdysone into *Drosophila* cells (Okamoto *et al.*, 2018b).

**Test for bloating larvae and statistics.** Late third instar larvae (120h AEL) were put in PBS and imaged under a microscope. We considered a 'bloating larvae' when they were inflated and we detected transparent regions that were usually filled with fat body content. Therefore, the % of bloating larvae was calculated after the number of larvae that showed this phenotype (n=200 for each genotype). For each sample we scored the percentage of individuals that belong to the "bloating larvae" category and calculated the standard error of sample proportion based on binomial distribution (bloating or not)  $SE = \sqrt{p(1-p)/n}$ , where p is the proportion of successes in the population. Volume was calculated using Fiji software.

**Water volume, hemolymph volume and dry mass.** We adapted the protocol to *Drosophila* larvae from the one described in Folk, Han and Bradley, 2001. Synchronized third instar larvae were first rinsed in PBS 1X and dried in a Kimwipe paper. Afterwards they were weighted in groups of 10 (total mass). Hemolymph was blotted out from the abdominal opening with a Kimwipe moistened with PBS1X. Each group of larvae were reweighted (total mass-hemolymph content), dried for 1 hour at 60°C and weighted a third time (dry mass). The water accumulation was computed by subtracting the dry mass from the wet mass. The hemolymph content was estimated by determining the reduction in mass following hemolymph blotting. The percentage of dry mass was calculated with the formula  $\text{dry mass} \times 100 / \text{wet mass}$ . Delta  $\Delta$  dry mass shows variation in total dry mass between control and tumor-bearing larvae. The delta between the two conditions is plotted as a single value. For each experiment, 5 replicates were carried out. P values were calculated after a one-way ANOVA with the Tukey-Kramer multiple comparisons test.

**Food intake.** Food intake was calculated as described in Bjordal *et al.*, 2014. Synchronized pre-wandering third instar larvae were washed in PBS 1X, dried on a Kimwipe and incubated for 3 hours at 25°C in a petri dish with regular food supplemented with 1,5% w/v of blue dye (Erioglaucine Disodium Salt, Sigma-Aldrich). Afterwards, larvae were washed again, dried and put together in groups of 8 in tubes to be frozen in liquid N<sub>2</sub>. Then they were transferred to a freezer at -20°C. Samples were homogenized in 20ul PBS 1X and centrifuged for 20 min at 4°C. 10ul were finally put in a new tube and the amount of blue dye in the supernatant was measured spectrophotometrically (OD<sub>629nm</sub>). Relative  $\Delta$  food intake shows variations in food intake according to different tumor-bearing larvae compared with their controls, respectively. The delta between the two conditions is plotted as a single value. P values were calculated after an ordinary one-way ANOVA test. The quantification of the mean larval weight was carried out

immediately after this protocol and P values were calculated after a one-way ANOVA with the Tukey-Kramer multiple comparisons test.

**Immunocytochemistry.** Immunostaining was performed using standard protocols. Primary antibodies used in this work are detailed in the KRT. Fluorescently labeled secondary antibodies were from Thermofisher Scientific. Larval tissues were mounted in Slowfade™ Diamond with DAPI (Thermofisher) and images were taken under an inverted Laser Scanning Confocal Microscope with Spectral Detection (LSM900 - Zeiss).

*Lysotracker Staining.* We followed the protocol described in Devorkin and Gorski, 2014. Fat bodies from third instar larvae were dissected in PBS and then incubated for 5 minutes in 100 µM LysoTracker Red DND-99 (Invitrogen) at RT. Then they were fixed in 4% paraformaldehyde for 30 minutes, washed in PBS and mounted in Slowfade™ Diamond (Thermofisher).

*Nile Red Staining.* Fat bodies from third instar larvae were dissected in PBS and immediately fixed in 8% paraformaldehyde for 45 minutes. They were washed twice in PBTween 0,1% and incubated for 5 minutes in diluted Nile Red Solution (1:8000 from 200µg/ml stock in DMSO, Sigma N3013) at RT. They were washed again in PBTween 0,1% and mounted in Slowfade™ Diamond (Thermofisher). Fiji software was used to quantify lipid droplets and droplet size.

*2-NBDG glucose analog staining.* The dye was reconstituted with 200µl RNAase-free water and kept at -20°C. Then fat bodies were incubated in 2-NBDG diluted 1:100 in PBX1X for 15 minutes in the dark, rinsed twice and fixed in 4% paraformaldehyde for 30 minutes at RT. Tissues were rinsed again and mounted in Prolong™ (Thermofisher).

**Quantitative RT-PCR.** Larvae were collected at the indicated time point AEL and specific tissues were dissected in cold PBS1X then frozen immediately in liquid N<sub>2</sub>. Total RNA was extracted using a QIAGEN RNeasy lipid tissue minikit or microkit according to the manufacturer's protocol. 2µg of each sample were treated with DNase I (Invitrogen) and reversely transcribed using a SuperScript II reverse transcriptase (Invitrogen). The resulting cDNA was utilized for quantitative qPCR (Viia 7; Applied Biosystems). cDNA was diluted 1:50 in H<sub>2</sub>O and mixed with 10uM primers and Power SYBR™ Green PCR Master Mix (Applied Biosystems). Samples were normalized to levels of *ribosomal protein (rp)49* transcript levels. Three separate biological samples were collected for each experiment and triplicate measurements were conducted. Primers used in this work are detailed in the key resources table.

**Pupariation curves.** 4h-egg laying's were carried out in small plates made of PBS 1X, 2% agar and 2% Glucose. After 24 hours first instar larvae were transferred to vials filled with standard fly food (40-50

larvae per tube) and let in an incubator at 25°C. The number of larvae that had pupariated at a given time AEL was scored at 114, 120, 128, 132, 140, 144, 152, 156 and 164 hours.

**Circulating ecdysone measurements.** 5ul of hemolymph for each genotype were homogenized and extracted in 200ul methanol. Extractions were then submitted to a competitive ELISA test as previously published (Rewitz, Yamanaka and O'Connor, 2010b) to evaluate the amount of circulating 20-E, using the detection kit from SpiBio (Bertin reagents) as recommended by the manufacturer. Absorbance at 415nm was detected using a TECAN microplate reader. Delta shows variation in circulating ecdysteroids normalized by the hemolymph volume between control larvae and the rest of the indicated genotypes. The delta is plotted as a single value.

**Trehalose and Glucose measurements.** For each genotype, synchronized first instar larvae were incubated at 25°C until early third instar. Three technical replicates of 1,5ul hemolymph were used for each condition. Hemolymph samples were diluted in 149ul test buffer TB (5mM Tris pH6.6, 137mM NaCl and 2.7mM KCl) and heated for 5 min at 70°C. Each sample was separated into two tubes of 70ul. 70ul of TB were added to one of the tubes and 70ul of trehalose buffer TbT (1mL TB + 3uL Porcine trehalase, Sigma, T8778-1UN) to the other. Trehalose and Glucose standards (1, 0,16, 0,08, 0,04, 0,02 and 0,01 mg/ml, Trehalose from Sigma 90208) were prepared in the same way. Both the samples and the standards were incubated at 37°C overnight. The next day tubes were centrifuged for 3 minutes and 30ul of each one was transferred to individual wells of a 96-well plate. 100ul of GO reagent (GAGO-20 Sigma) were put on and then the plate was sealed and incubated at 37°C for 30 to 60 minutes. To stop the reaction, 100ul of sulfuric acid were added. Absorbance at 540nm was detected using a TECAN microplate reader. Concentration was calculated based on the equation given by a linear regression and the dilution. P values were calculated after an ordinary one-way ANOVA test.

**Ex-vivo incubation of fat bodies.** Fat bodies from tGPH larvae with indicated genotypes were incubated for 30 minutes at RT in Schneider's medium with or without human insulin (0,5uM #I9278 Sigma). Incubation mix was then removed and tissues were fixed and processed as described above. Chicken anti-GFP antibody (1:10000, Abcam) was used as primary. Images were obtained under an inverted Laser Scanning Confocal Microscope with Spectral Detection (LSM900 - Zeiss) and processed with Fiji Software. Delta tGPH shows variation in membrane tGPH between fat bodies from the same larvae incubated with or without insulin. The delta between the two conditions is plotted as a single value. P values were calculated after a one-way ANOVA with the Tukey-Kramer multiple comparisons test.

**Preparation of *erg2Δ::Trp1* yeast food.** Fly food made of *erg2Δ::Trp1* yeast was prepared as previously described (Katsuyama and Paro, 2013).

*Yeast culture.* A synthetic complete tryptophan-minus medium was prepared and autoclaved (6.7g yeast nitrogen base without amino acids BD DIFCO 291940, 5g Cassamino acids BD Bacto 223050, 20g Glucose Sigma G7021 and 1L milliQ water). 10ml of 100X Uracil were added and the *erg2Δ::Trp1* yeast was inoculated and cultured at 37°C until reaching an  $OD_{600nm}=1$ . Then the harvested cells were centrifuged and washed several times with PBS and the clean 10ml yeast pellet was immediately used or stored frozen until used.

*erg2Δ food preparation.* The frozen 10ml yeast pellet was suspended in 10ml PBS 1X and boiled for 30 minutes. Then the heat-inactivated yeast paste was mixed with 0.1g glucose, 0.12 agar, 10 ml water and 300ul of propionic acid under sterilized conditions. The food was distributed in vials (5ml per vial).

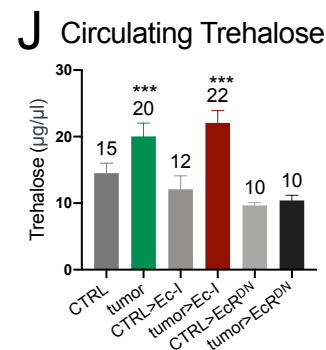
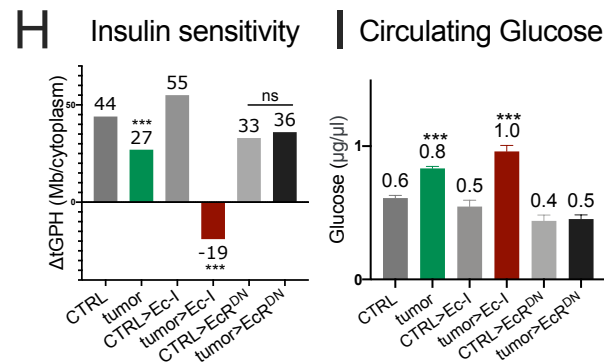
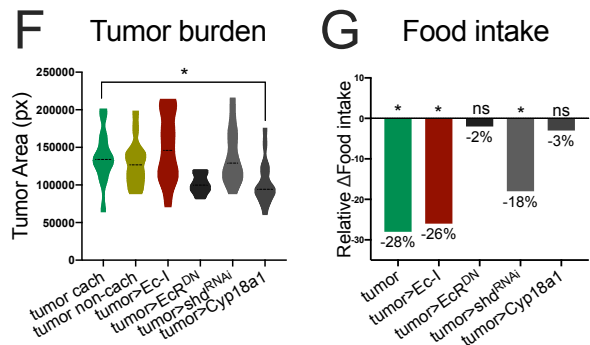
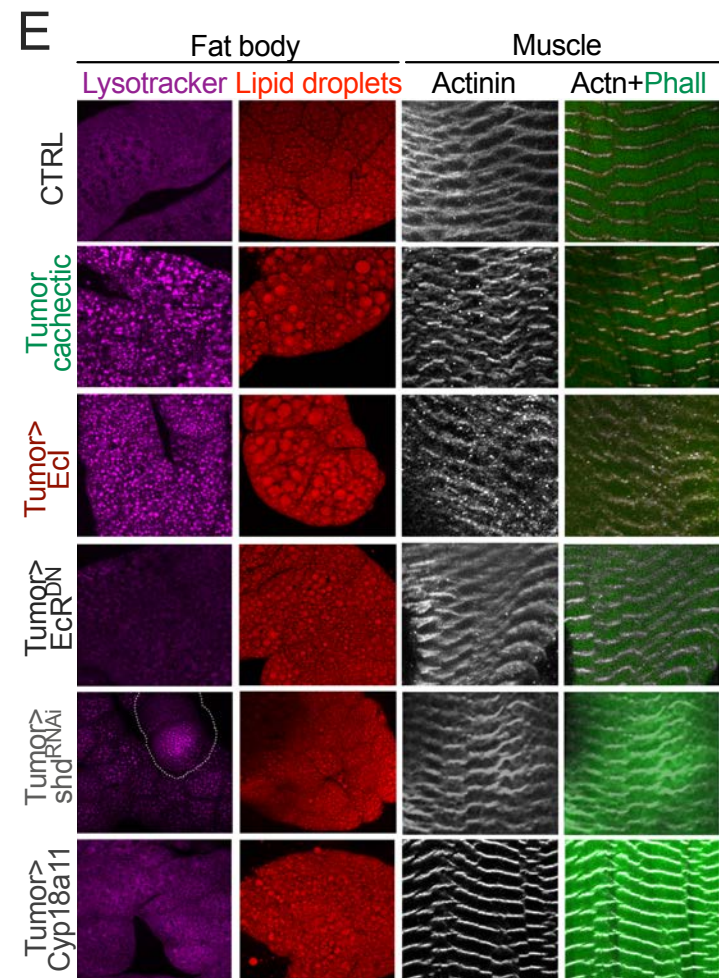
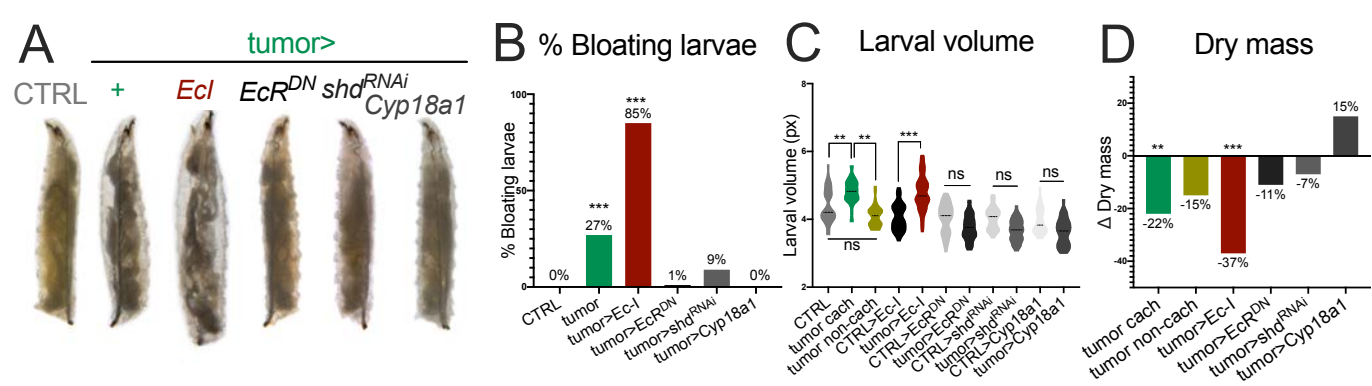
*erg2Δ food experimental conditions.* Staged embryos were sterilized with 3% sodium hypochlorite solution, washed twice in PBS 1X and transferred to vials with the help of a sterilized net (around 25 eggs per vial). The tubes were transferred to a 25 degrees chamber and larvae were analyzed at specific time points (120h AEL).

**20-E treatment.** 4h-egg laying were carried out in small plates made of PBS 1X, 2% agar and 2% Glucose. After 24 hours first instar larvae were transferred to vials filled with standard fly food (40-50 larvae per tube) and let in an incubator at 25°C. At 48, 72 and 96h AEL, 100ul of a 0,2mg /ml ethanol of 20-E (Sigma, H5142) fresh solution were added, and larvae were analyzed at 120h AEL. In parallel, we added the same quantity of ethanol to control tubes.

**Binding site prediction.** *Oatp33Eb* genomic sequence was taken from the NCBI reference sequences collection (RefSeq). Putative Binding sites were analyzed in JASPAR database (<http://jaspar2016.genereg.net/>) using the EcR::Usp matrix model (MA0534.1, Uniprot ID: P34021 P20153 , PubMed ID 8649409) with a Relative profile score threshold of 80%.

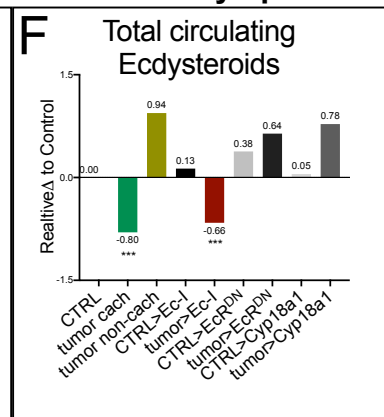
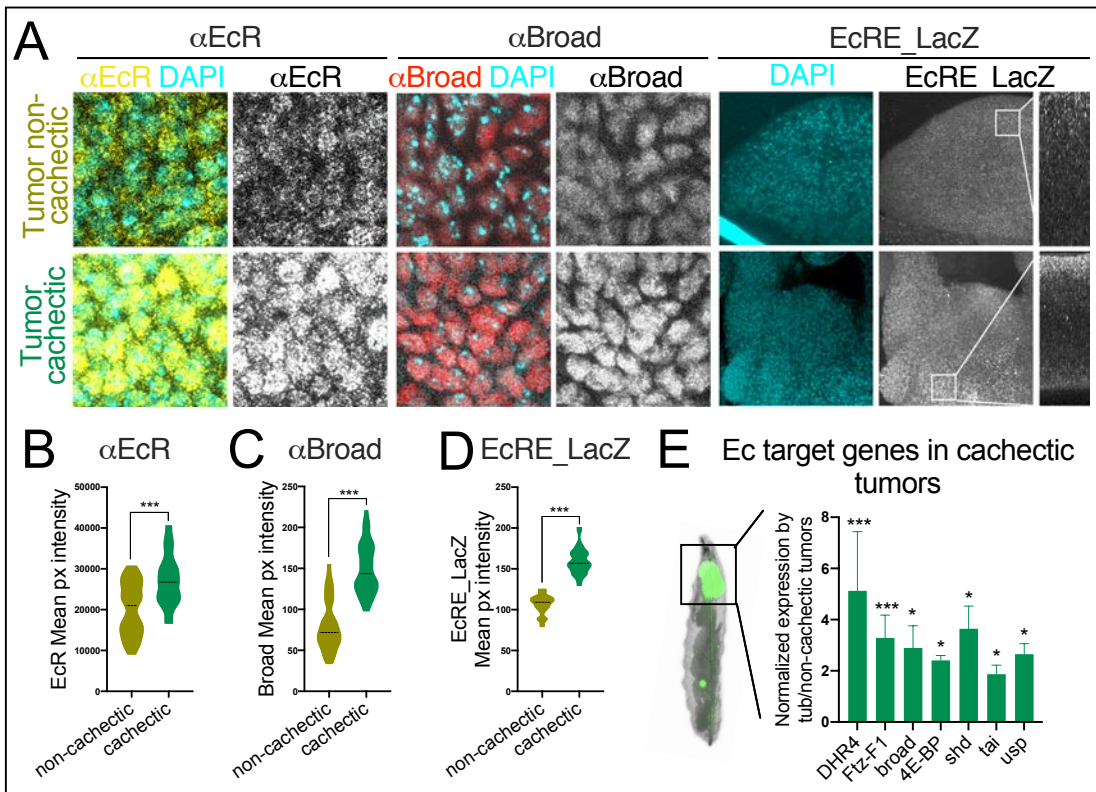
## QUANTIFICATION AND STATISTICAL ANALYSIS

Statistical analyses were performed with GraphPad Prism V8 and Microsoft Excel. For each experimental condition, control samples were carried out in parallel with the same set-up and both the software and the statistical test used to compare them are detailed in the methods section. For each graph, the mean values, statistical errors, p-values and n numbers are described in the corresponding figure legend.

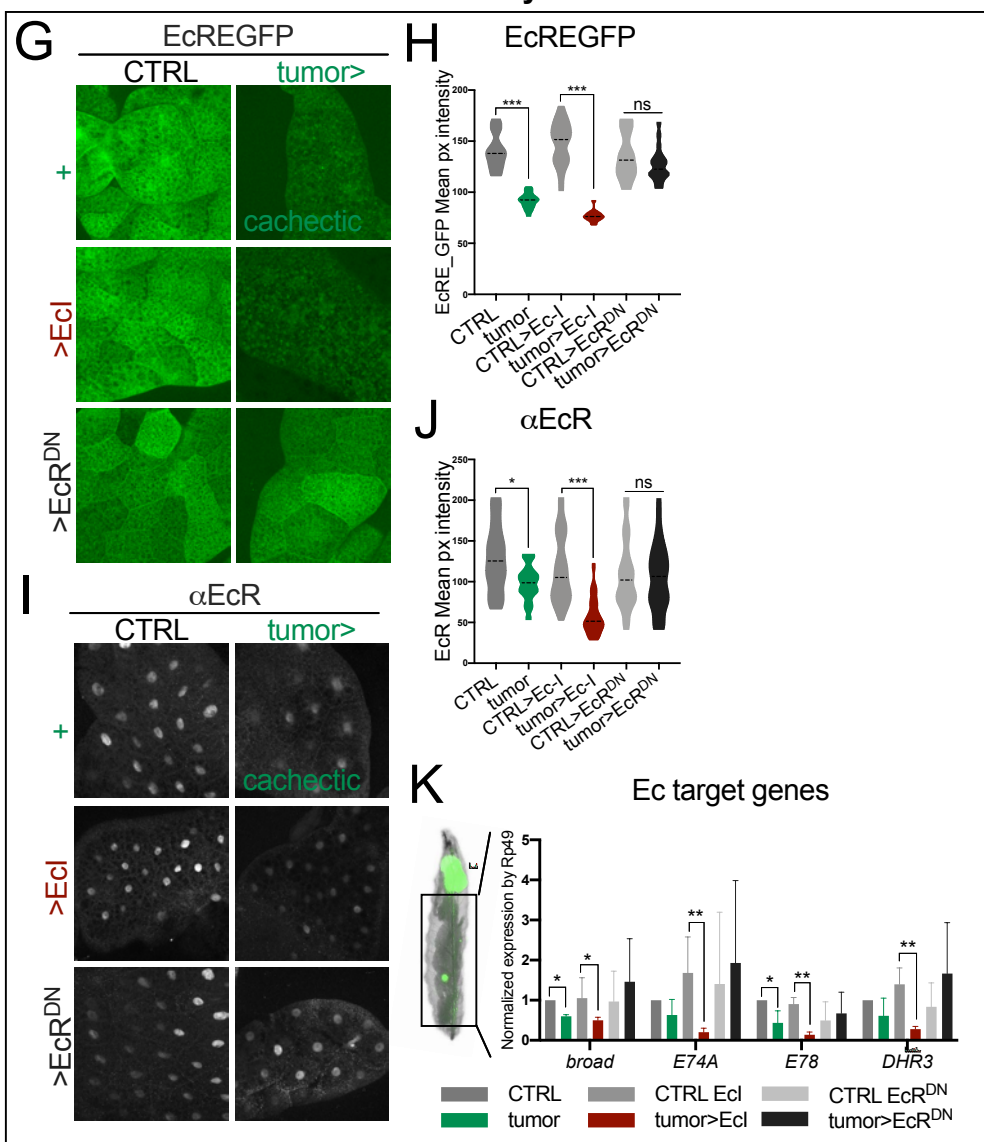


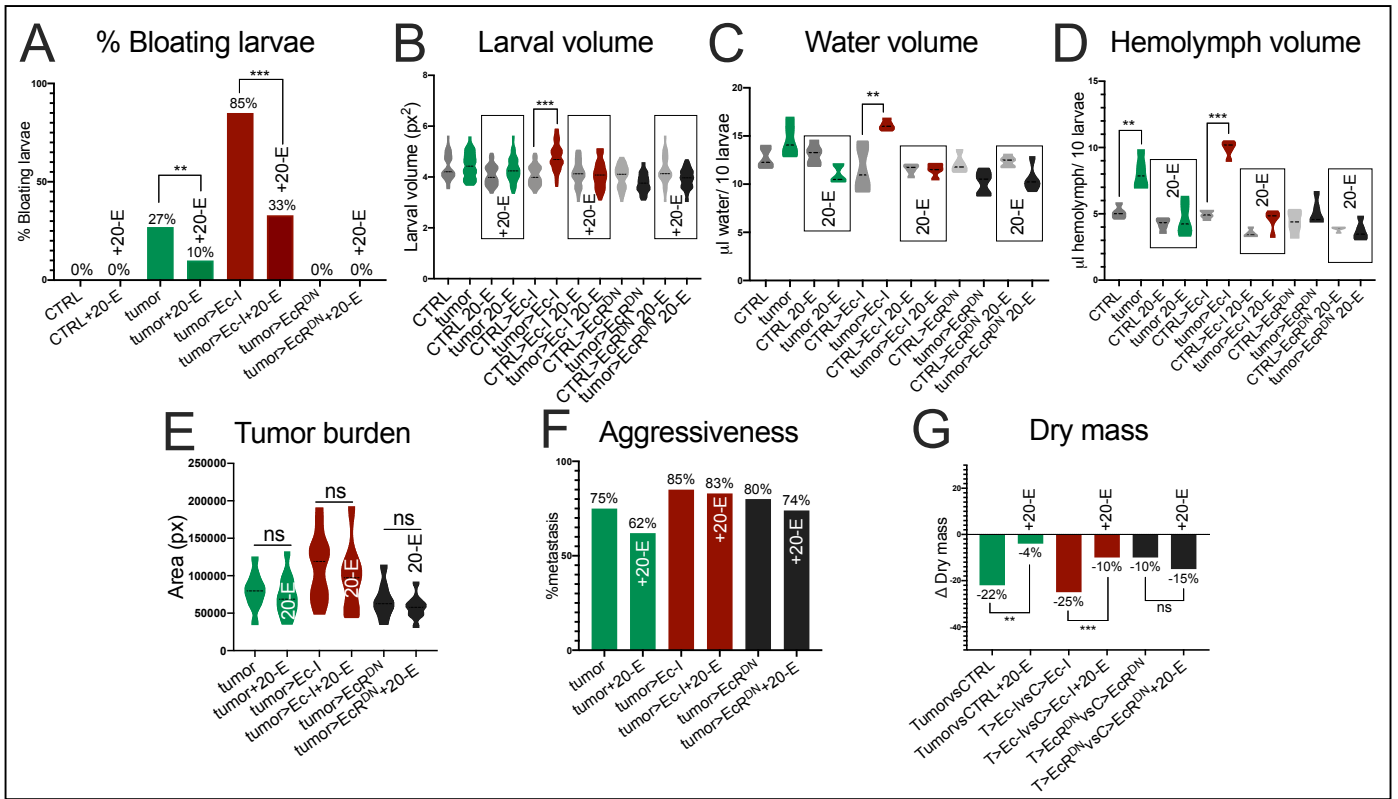
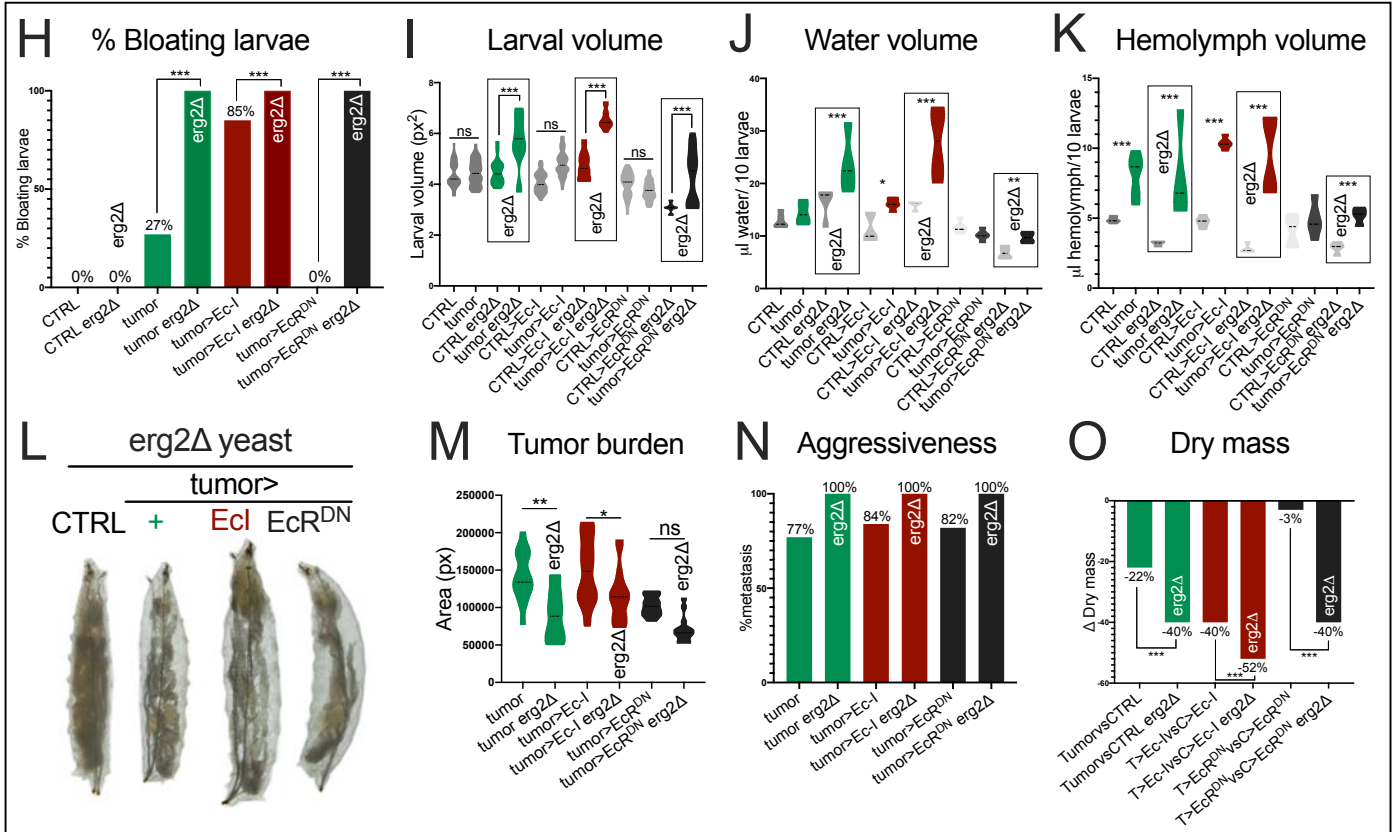
## Tumor

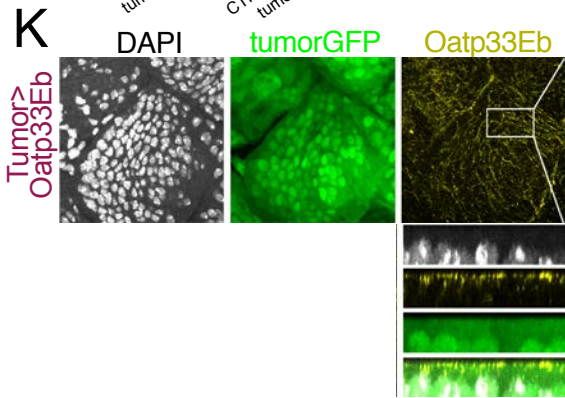
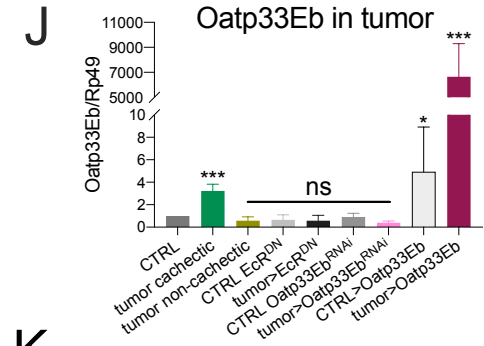
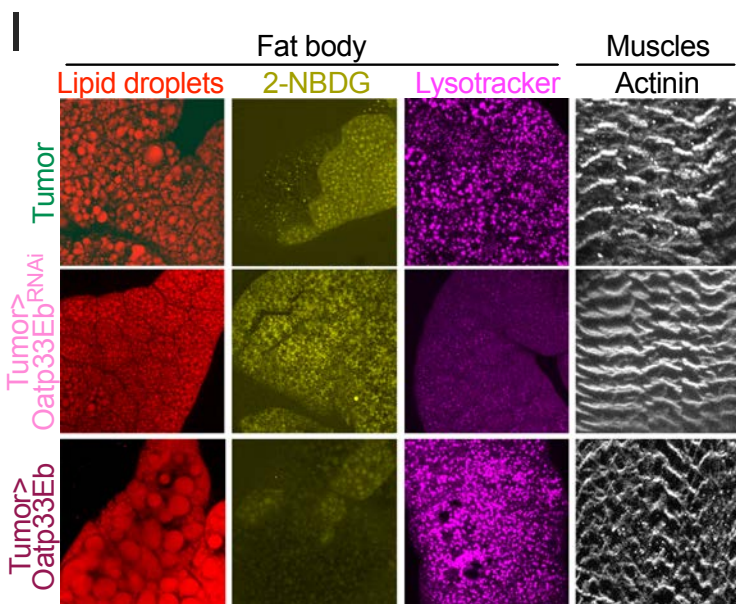
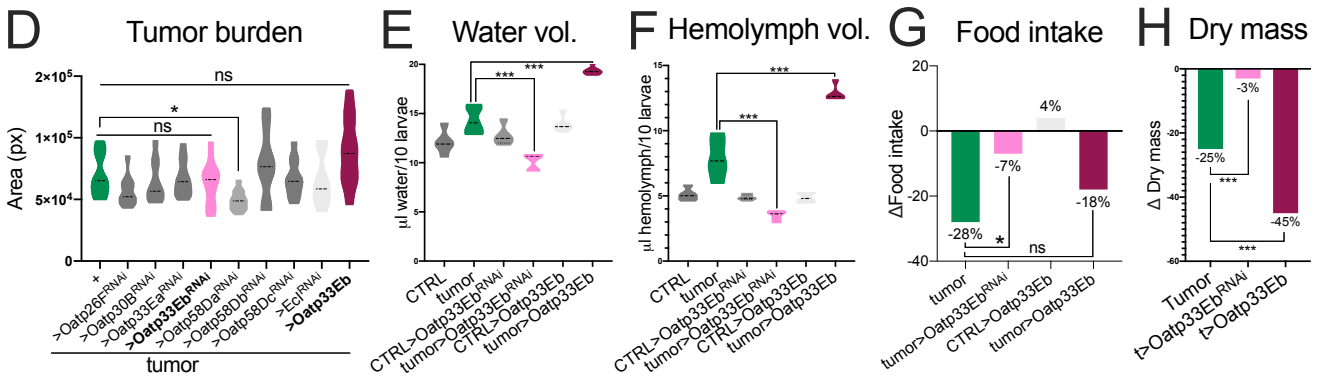
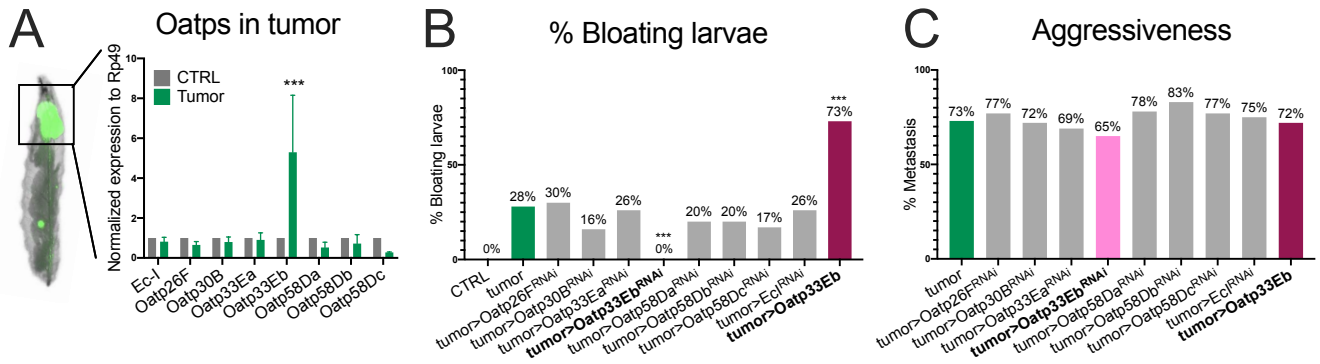
## Hemolymph



## Fat body



**+20-E****erg2Δ**





Control larvae

Tumor-bearing larvae

